



HAL
open science

E-site drug specificity of the human pathogen *Candida albicans* ribosome

Yury Zgadzay, Olga Kolosova, Artem Stetsenko, Cheng Wu, David Bruchlen, Konstantin Usachev, Shamil Validov, Lasse Jenner, Andrey Rogachev, Gulnara Yusupova, et al.

► **To cite this version:**

Yury Zgadzay, Olga Kolosova, Artem Stetsenko, Cheng Wu, David Bruchlen, et al.. E-site drug specificity of the human pathogen *Candida albicans* ribosome. *Science Advances*, 2022, 8 (21), pp.eabn1062. 10.1126/sciadv.abn1062. hal-03813407

HAL Id: hal-03813407

<https://hal.science/hal-03813407>

Submitted on 13 Oct 2022

HAL is a multi-disciplinary open access archive for the deposit and dissemination of scientific research documents, whether they are published or not. The documents may come from teaching and research institutions in France or abroad, or from public or private research centers.

L'archive ouverte pluridisciplinaire **HAL**, est destinée au dépôt et à la diffusion de documents scientifiques de niveau recherche, publiés ou non, émanant des établissements d'enseignement et de recherche français ou étrangers, des laboratoires publics ou privés.

STRUCTURAL BIOLOGY

E-site drug specificity of the human pathogen *Candida albicans* ribosome

Yury Zgadzay^{1,2†}, Olga Kolosova^{1†}, Artem Stetsenko³, Cheng Wu⁴, David Bruchlen¹, Konstantin Usachev^{2,5}, Shamil Validov^{2,5}, Lasse Jenner¹, Andrey Rogachev^{6,7}, Gulnara Yusupova¹, Matthew S. Sachs⁴, Albert Guskov^{3,6*}, Marat Yusupov^{1,2,5*}

Candida albicans is a widespread commensal fungus with substantial pathogenic potential and steadily increasing resistance to current antifungal drugs. It is known to be resistant to cycloheximide (CHX) that binds to the E-transfer RNA binding site of the ribosome. Because of lack of structural information, it is neither possible to understand the nature of the resistance nor to develop novel inhibitors. To overcome this issue, we determined the structure of the vacant *C. albicans* 80S ribosome at 2.3 angstroms and its complexes with bound inhibitors at resolutions better than 2.9 angstroms using cryo-electron microscopy. Our structures reveal how a change in a conserved amino acid in ribosomal protein eL42 explains CHX resistance in *C. albicans* and forms a basis for further antifungal drug development.

INTRODUCTION

Candida albicans is a pathogenic yeast that frequently causes potentially lethal infections (1). There are several classes of antifungal drugs that combat candidiasis; however, most of them have numerous side effects and are expensive, and there is a steady increase in cases of *C. albicans* infections that are drug resistant (2). None of these drugs target the protein synthesis apparatus—the ribosome, which is a very successful route to combat prokaryotic pathogens (3). Bioinformatics analysis suggests that the structural organization of functional sites of the *C. albicans* ribosome should be highly similar to the *Saccharomyces cerevisiae* and *Homo sapiens* ribosomes (4). Nevertheless, there are several key positions in ribosomal RNA (rRNA) and ribosomal proteins at which nucleotide or amino acid substitutions can modulate specific features of the translation cycle and determine resistance to specific inhibitors (5). *C. albicans* is resistant to cycloheximide (CHX) (6), which binds to the ribosomal E-tRNA binding site (E-site) (7). Genetic studies have demonstrated that this resistance is most likely caused by a natural substitution, P56Q, in ribosomal protein eL42 (8). However, the mechanistic basis for this has not been determined by direct structural methods.

For the rational design of drugs targeting the *C. albicans* ribosome but not human ribosomes, an understanding of drug-target interactions in the context of the structure of the *C. albicans* ribosome is indispensable. Therefore, we investigated the structural determinants of ribosomal functional sites, including the E-site and the peptidyl transferase center (PTC), of the *C. albicans* ribosome as potential targets for antifungal drug development. Here, we present cryo-electron microscopy (cryo-EM) structures of the vacant *C. albicans* ribosome and its complexes with four known eukaryotic

inhibitors, namely, CHX, phyllanthoside (PHY), anisomycin (ANM), and blasticidin S (BLS). These studies reveal structural differences in the *C. albicans* E-site compared to the *S. cerevisiae* and *H. sapiens* ribosomes that affect CHX binding, which we propose could be exploited for the development of selective translational inhibitors.

RESULTS AND DISCUSSION

Previously, we have studied the structural organization of the E-site of the 60S subunit of *S. cerevisiae* ribosome by determining complexes with a CCA-end analog of tRNA and E-site inhibitors (9). It was shown that the rRNA in this pocket is highly conserved between yeasts and humans and is responsible for most interactions with inhibitors. Along with rRNA in the E-site, eukaryote-specific ribosomal protein eL42 interacts with some inhibitors and stabilizes them in the binding pocket (10). Here, in the determined structure of the vacant *C. albicans* ribosome, a strong density for a domain of the E-site tRNA was observed, although it was not introduced exogenously (fig. S1F). The presence of endogenous E-site tRNA is not a unique feature of the *C. albicans* ribosome but has been observed for isolation of ribosomes from many other species. Further comparison of the vacant *C. albicans* ribosome with the ribosomes from *S. cerevisiae* and from *H. sapiens* revealed that in the E-site of *C. albicans* ribosome, there is a P56Q alteration in ribosomal protein eL42 (fig. S1A). This is the only difference found in the organization of the functional sites between *C. albicans*, *S. cerevisiae*, and *H. sapiens* (table S1).

The eL42 P56Q substitution decreases the volume of the binding pocket. To establish whether the reduction of the pocket volume affects the binding of inhibitors, we compared the *S. cerevisiae* ribosome [Protein Data Bank (PDB) 4U3U] and *H. sapiens* (PDB 5LKS) ribosome in complex with CHX (fig. S3A) to the vacant *C. albicans* ribosome (at 2.3 Å) with a superimposed CHX molecule. CHX binds to the 60S subunit in the E-site, preventing translocation of tRNA from P- to E-site (Fig. 1A). In *S. cerevisiae*, CHX forms five hydrogen bonds with 25S rRNA specifically with G92, C93, U2763, and C2764 (*C. albicans* G91, C92, U2735, and C2736). The main difference between the two species concerning CHX binding is the lack of interaction of CHX with P56 of eL42 in *S. cerevisiae*, where

Copyright © 2022
The Authors, some
rights reserved;
exclusive licensee
American Association
for the Advancement
of Science. No claim to
original U.S. Government
Works. Distributed
under a Creative
Commons Attribution
NonCommercial
License 4.0 (CC BY-NC).

¹Department of Integrated Structural Biology, Institute of Genetics and Molecular and Cellular Biology, University of Strasbourg, Illkirch, France. ²Laboratory of Structural Biology, Institute of Fundamental Medicine and Biology, Kazan Federal University, Kazan, Russia. ³Groningen Biomolecular Sciences and Biotechnology Institute (GBB), University of Groningen, Groningen, Netherlands. ⁴Department of Biology, Texas A&M University, College Station, TX, USA. ⁵Federal Research Center "Kazan Scientific Center of Russian Academy of Sciences", Kazan, Russia. ⁶Moscow Institute of Physics and Technology, Dolgoprudny, Russia. ⁷The Joint Institute for Nuclear Research, Dubna, Russia.

*Corresponding author. Email: a.guskov@rug.nl (A.G.); marat@igbmc.fr (M.Y.)

†These authors contributed equally to this work.

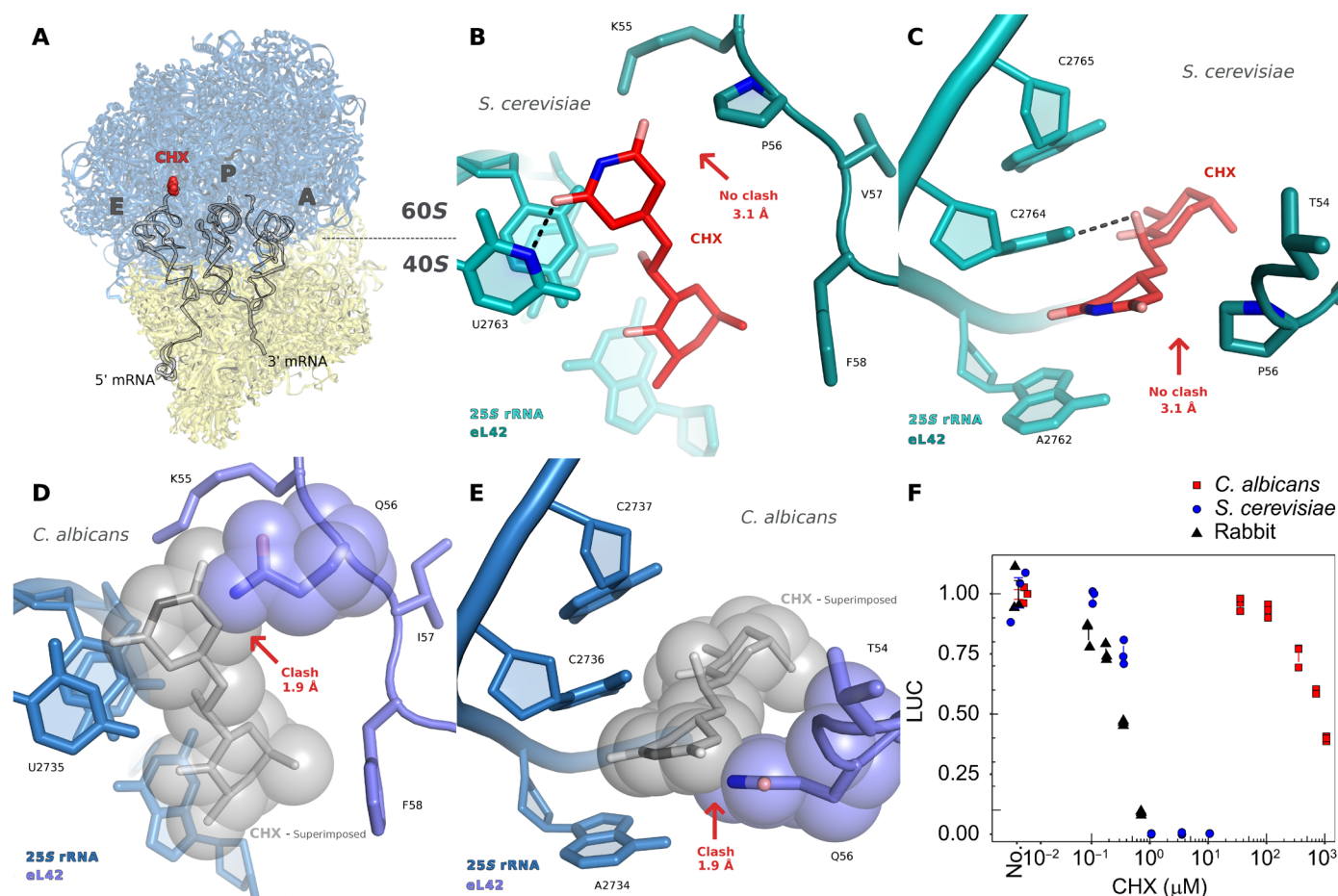


Fig. 1. Q56 prevents binding of CHX to the *C. albicans* ribosome. (A) Overview of the CHX binding site (red) in the *C. albicans* 80S ribosome. The 40S subunit is shown in yellow, the 60S subunit is shown in blue, and mRNA and tRNA are shown in gray. The CHX molecule was superimposed from *S. cerevisiae* ribosome (PDB 4U3U), and mRNA and tRNAs were superimposed from the *Thermus thermophilus* (PDB 4V4Y). (B and C) Binding of CHX to the *S. cerevisiae* ribosome shown in two orientations (PDB 4U3U) (9). (D and E) Close-up views of the *C. albicans* CHX binding site in two orientations. The glutarimide group of CHX clashes with the side chain of Q56 preventing CHX from binding to the ribosome of *C. albicans*. (F) Inhibition of translation by CHX in cell-free translation extracts (CFTS) from *C. albicans*, *S. cerevisiae*, and rabbit reticulocytes. Cell-free experiments were performed twice using independent technical triplicates; the results of one set of triplicates are shown. The root mean square deviation of luciferase (LUC) activity was 2 to 5%.

the CHX molecule is 3.1 Å distant from the proline side chain (Fig. 1, B and C). Superimposing CHX into the vacant *C. albicans* ribosome creates a clash between the Q56 side chain and the glutarimide group of CHX (Fig. 1, D and E). Our findings suggest that electrostatic repulsion between O ϵ oxygen of the glutamine side chain and O6 oxygen of CHX occludes its binding to the *C. albicans* ribosome.

Cell-free assays and microplate drug inhibition (MIC) experiments corroborated this finding. Translation of sea pansy luciferase (spLUC) in the *C. albicans* cell-free translation extract (CFTS) is approximately 1000-fold more resistant to CHX than the *S. cerevisiae* and the rabbit reticulocyte CFTSs (Fig. 1F). In MIC assays, 100% inhibition of *S. cerevisiae* growth was obtained with 1 μM CHX. In contrast, approximately 67% inhibition of *C. albicans* growth was observed with 900 μM CHX, and limited growth was still observed with 7 mM CHX (fig. S2).

On the basis of CFTS assays, we attempted to bind CHX at high excess in nonphysiological conditions (≥ 1 mM) to understand possible rearrangements in the E-site upon the inhibitor binding.

Only at 1 mM was density for CHX observed in the E-site (fig. S3B). The quality of the map allowed for visualization of the ribosome structural rearrangement upon CHX binding (Fig. 2A). We found that, in *C. albicans*, the CHX molecule adopts a different conformation, not penetrating so deep as in *S. cerevisiae* and in *H. sapiens*. By comparing CHX binding with the vacant ribosome with superimposed CHX, a 1-Å shift of the whole CHX molecule was observed (Fig. 2B). To bind to the E-site at a high concentration, the CHX molecule pushes the Q56 side chain 1.4 Å downward (Fig. 2C). Consequently, there is a slight shift in positions of the C2736, C2737, and G2766 with a 12° rotation of U2735 in comparison to the vacant *C. albicans* ribosome structure. In addition, a slight shift of the eL42 protein backbone is observed. These observations corroborate that there is no high-affinity binding site for CHX in the *C. albicans* ribosome.

While many inhibitors that target the E-site are known, most of them have a glutarimide group, which prevents their binding to the *C. albicans* ribosome at physiological concentrations (4). Only one known E-site inhibitor, PHY (fig. S3C), does not have a glutarimide

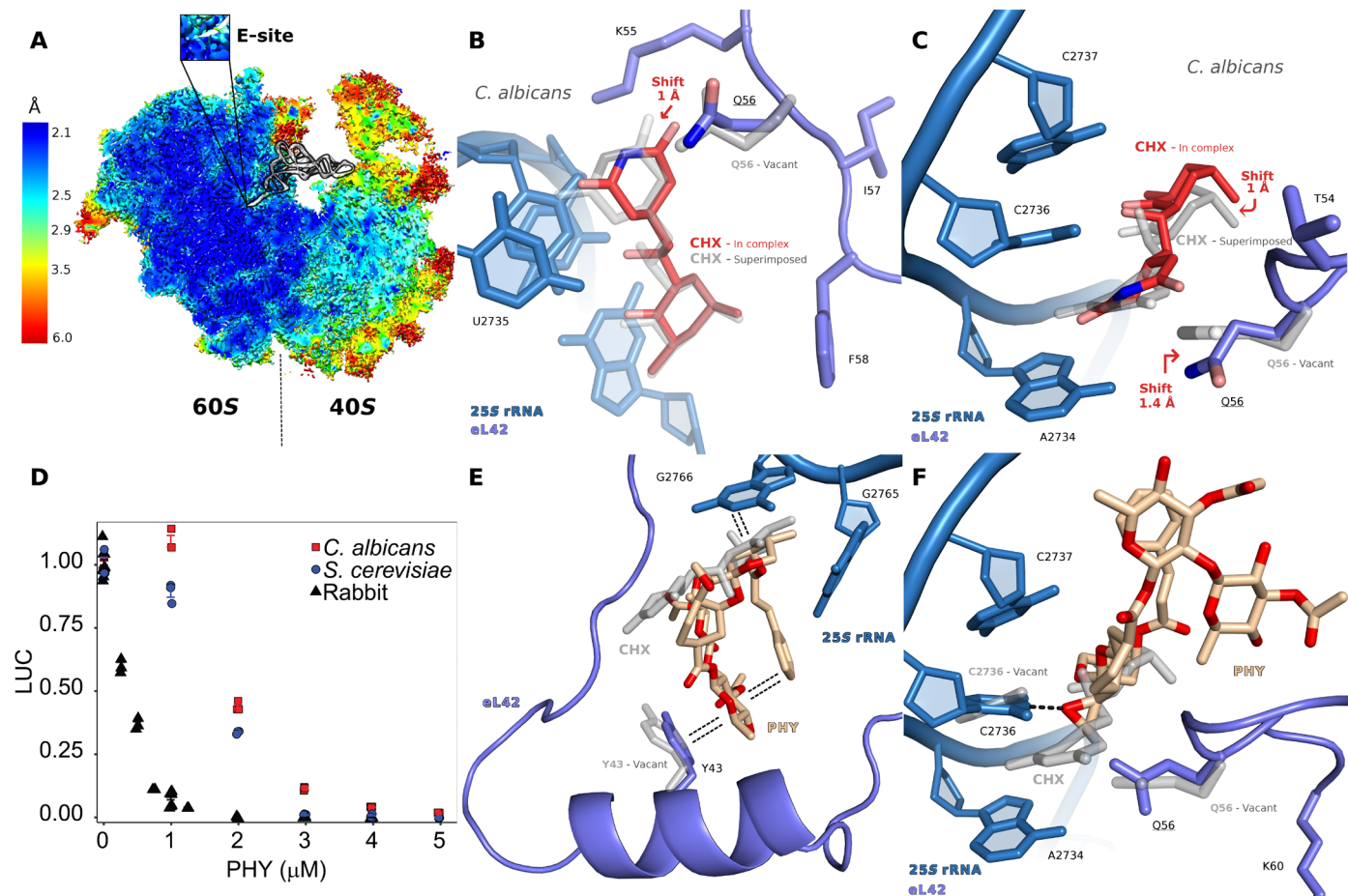


Fig. 2. CHX and PHY binding to the *C. albicans* ribosome. (A) Local resolution map of the *C. albicans* ribosome with the close-up view onto the E-site. (B and C) CHX adopts a different conformation in comparison with the superimposed molecule. Low-affinity binding of CHX leads to movement of the Q56 side chain. (D) Effect of PHY on translation in cell-free systems from *C. albicans*, *S. cerevisiae*, and rabbit reticulocytes. Cell-free experiments were performed twice using independent technical triplicates; the results of one set of triplicates is shown. The root mean square deviation of LUC activity was 2 to 5%. (E and F) Overview of PHY binding site. PHY interacts with Y43 of the eL42 and with 25S rRNA forming a hydrogen bond with C1736.

moiety and thus could be active against *C. albicans*. To test this hypothesis, we performed cell-free translation experiments in the presence of PHY. In notable contrast to CHX, translation of spLUC in all three species was similarly sensitive to PHY (Fig. 2D). To corroborate this finding, we determined the cryo-EM structure of the *C. albicans* ribosome in complex with PHY (100 μM concentration) at 2.6-Å resolution. The obtained map revealed a strong density in the E-site that corresponds to PHY (fig. S3D), which binds in a manner resembling the tRNA CCA-end. It forms two stacking interactions with G2766 of 25S rRNA and Y43 of eL42 (Fig. 2E). Because of the lack of a glutarimide group, PHY does not clash with Q56, in contrast to the situation with CHX (Fig. 2F). The epoxide group of PHY, which is the closest to Q56, is located 5.3 Å away from that residue. However, this group is very close to C2735 (2 Å) and has previously been suggested to form a covalent bond with C2736 (C2764 in *S. cerevisiae*), which results in an irreversible inhibitory effect on protein synthesis (9). In addition, we found that, with PHY in the E-site, U2735, C2736, G2765, and G2766 slightly changed their conformation compared to the structure of the vacant ribosome (Fig. 2F). Despite the direct interaction (stacking) with eL42 Y43 (Fig. 2E), PHY causes a 0.65-Å shift of the eL42

backbone (residues K55 to K60; Fig. 2F) similar to what was observed in the *S. cerevisiae* structure (PDB 4u4z). In addition, density for the E-site tRNA was not detected, indicating that PHY's binding prevents tRNA entry into the E-site (fig. S4). These structural results suggest that PHY is the only currently known E-site inhibitor of *C. albicans*. Although this inhibitor cannot discriminate between *C. albicans* and other eukaryotic ribosomes, it can serve as a starting point for the rational drug design of a specific inhibitor.

In addition, we found a strong density for a spermidine molecule in the E-site close to uL15, although spermidine was not introduced exogenously. This has previously been observed in *Neurospora crassa* (11) and in *S. cerevisiae* (12), but, here, we propose a structural role of spermidine for the E-site pocket formation. The spermidine molecule interacts with Q38 and H39, stabilizing the E-site binding pocket, although no hydrogen bonds are formed (fig. S5). We suggest that spermidine is the key factor to explain CHX resistance arising from mutations at residues Q38 and H39 of ribosomal protein uL15 (see Supplementary Text and fig. S5).

Additional differences of interest arising from the comparison between *C. albicans* and *S. cerevisiae* were also found. These differences could potentially be important for drug specificity at other

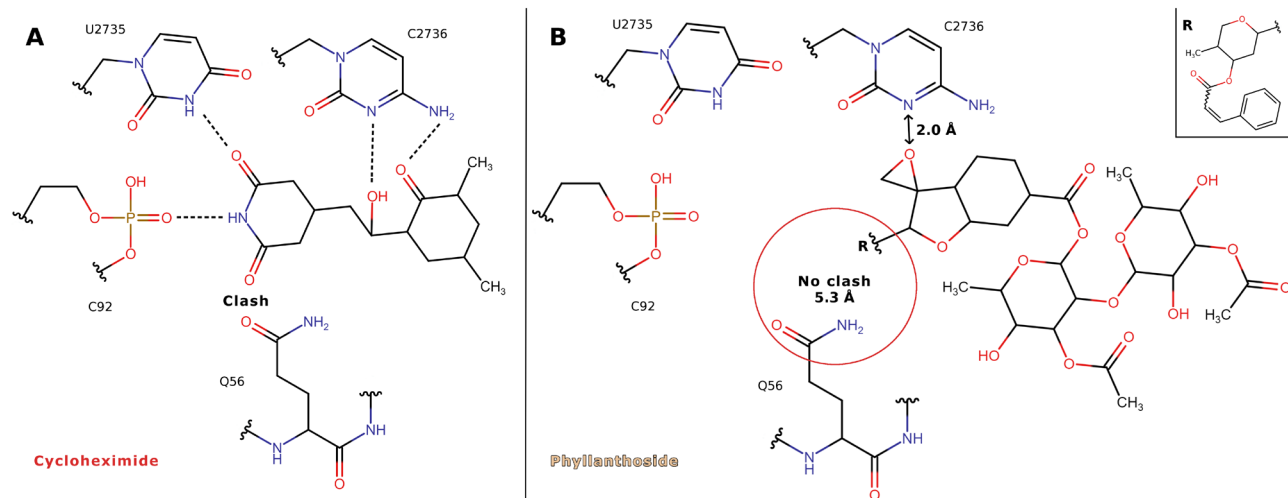


Fig. 3. E-site specificity of the *C. albicans* ribosome. (A) Schematic interaction of CHX binding to the E-site. CHX could not bind to the E-site of *C. albicans* due to the clash between the glutarimide group of CHX and Q56 side chain. (B) Schematic interaction of PHY binding to the E-site. PHY is the only E-site inhibitor that binds to *C. albicans* ribosome at physiological concentration. Because of the lack of glutarimide moiety, PHY does not clash with the Q56 located 5.3 Å apart.

functional sites of the ribosome. The PTC nucleotide composition of *C. albicans*, *S. cerevisiae*, and *H. sapiens* is identical (table S1). Nevertheless, in the *C. albicans* vacant ribosome, we found that 2793C and U2847 adopt different conformations compared to the vacant yeast ribosome (PDB 4v88). To understand whether these differences play any physiological role or might arise from differences in sample analyses (single particles versus crystal), structures of the *C. albicans* ribosome with an added ANM and BLS were determined (see Supplementary Text and figs. S3, E to H, and S6). No substantial differences in the binding site geometry and inhibitor interactions were observed when comparing ANM and BLS interactions with *C. albicans* and *S. cerevisiae* ribosomes. Consistent with the observed similarity of the binding of the A-site inhibitor ANM and the P-site inhibitor BLS to the *C. albicans* and *S. cerevisiae* ribosomes, inhibition of translation by these compounds was also similar in translation extracts from these two yeasts (fig. S6, C and E). Hence, it seems that the minor structural changes do not affect the binding or action of these inhibitors in the PTC.

In addition to the structural features of the PTC (fig. S1B), a high-quality map enabled us to find different conformations and modifications of proteins and rRNAs. About 60 amino acids with multiple side-chain conformations were observed, as well as three amino acids (lysines) with side-chain monomethylation, and 138 possible rRNA modifications (116 in 25S and 22 in 18S rRNAs) (fig. S1, C to E). While eL41 is not currently annotated in *Candida* species, eL41 protein was evident in the experimental density. A conserved DNA sequence in the genome of *C. albicans* SC5314 between orf19.1676 and orf19.1677 was identified with the help of curators at the *Candida* Genome Database (13) that specifies a 25-residue polypeptide similar to *S. cerevisiae* eL41 that fits into the density and therefore appears to be *C. albicans* eL41 (fig. S7).

A 2.32-Å [at FSC (Fourier shell correlation) = 0.143] high-resolution ribosome structure of one of the most pathogenic fungi, *C. albicans*, is reported. Our results explain the resistance of *C. albicans* to CHX and demonstrate specific features of the *C. albicans* ribosome. On the basis of structural and cell-free translation data, we propose that CHX cannot bind to the *C. albicans*

ribosome due to the clash of the glutarimide group of CHX with the Q56 side chain of eL42 (Fig. 3A). In contrast to CHX, PHY binds to the E-site of *C. albicans* at a physiologically relevant concentration. Because of the lack of the glutarimide moiety, PHY adopts an entirely different interaction pattern and does not clash with Q56 (Fig. 3B). Our study provides a solid base for potential future development of anti-*Candida* drugs without a glutarimide moiety that could lead to specific binding to the ribosome of *C. albicans*. Understanding ribosome inhibition will significantly improve the treatment of candidiasis and reduce the mortality associated with it.

MATERIALS AND METHODS

Materials

ANM, BLS, and CHX were purchased from Sigma-Aldrich. These compounds were dissolved in water because of their sufficient solubility at low concentrations (5 to 10 mM). PHY was provided by the National Institutes of Health Development Therapeutics Program and dissolved in dimethyl sulfoxide (54 mM).

Ribosome purification

80S ribosomes from *C. albicans* SC5314 were purified as described earlier, with minor changes (4). The *C. albicans* SC5314 strain was provided by S. Znaidi (Institut Pasteur, Paris, France). *Candida* cells grew in flasks to an OD₆₀₀ (optical density at 600 nm) of 1.0 in yeast extract–peptone–dextrose (YPD) medium at 30°C. Cells were pelleted by centrifugation, resuspended with YP, and incubated in flasks with vigorous shaking (250 rpm) for 10.5 min. Cells were precipitated and washed three times in buffer M [30 mM Hepes-KOH (pH 7.5) at room temperature, 50 mM KCl, 10 mM MgCl₂, 8.5% mannitol, 2 mM dithiothreitol (DTT), and 0.5 mM EDTA]. Following the final centrifugation (3450g for 10 min), the pellet was weighed. Typically, we obtained 5.5 g of cells from 4 liters of cell culture.

For 5.5 g of cells, the pellet was resuspended in 8 ml of buffer M and supplemented with additional 1500 μl from a solution of one complete protease inhibitor tablet (without EDTA, Roche) dissolved in 2 ml of buffer M, 250 μl of RNasin (Promega), 300 μl of

100 mM Pefabloc, 80 μ l of heparin (100 mg/ml), 30 μ l of 1 M DTT, and 650 μ l of 2 M KCl (concentration adjusted to 130 mM to precipitate lipids after breaking cells). The cell suspension was transferred to a round-bottom 50-ml tube (Nalgene) with 16.5 g of glass beads (Sigma-Aldrich). Cells were mechanically disrupted nine times on a vortex at a frequency of 40 Hz for 1 min with 1-min breaks on ice between each shake.

Beads were removed by short centrifugation (20,000g for 2 min), and the lysate was further clarified by a longer centrifugation (30,000g for 9 min). Polyethylene glycol (PEG) 20,000 was then added from a 30% (w/v) stock (Hampton Research) to a final concentration of 4.5% (w/v), and the solution was left to stand for 5 min on ice. The solution was clarified by centrifugation (20,000g for 5 min), and the supernatant was transferred to a new tube. Then, PEG 20,000 concentrations were adjusted to 8.5%, and the solution was left to stand for 10 min on ice. Ribosomes were precipitated (17,500g for 10 min), the supernatant was discarded, and residual solution was removed by a short spin of the pellet (14,500g for 1 min). Ribosomes were suspended (8 to 10 mg/ml) in buffer M+ (buffer M with KCl concentration adjusted to 150 mM and supplemented with protease inhibitors and heparin).

Ribosomes were further purified by a 10 to 30% sucrose gradient in buffer S [20 mM Hepes-KOH (pH 7.5), 120 mM KCl, 8.3 mM MgCl₂, 2 mM DTT, and 0.3 mM EDTA] using the SW28 rotor (18,000 rpm for 15 hours). The appropriate fractions were collected; KCl and MgCl₂ concentrations were adjusted to 150 and 10 mM, respectively; PEG 20,000 was then added to a final concentration of 7% (w/v); and the solution was left to stand 10 min on ice. Ribosomes were precipitated (17,500g for 10 min), the supernatant was discarded, and residual solution was removed by a short spin of the pellet (17,500g for 1 min). Ribosomes were suspended (25 mg/ml) in buffer G [10 mM Hepes-KOH (pH 7.5), 50 mM KOAc, 10 mM NH₄OAc, 2 mM DTT, and 5 mM Mg(OAc)₂]. Typically, 14 to 16 mg of pure ribosomes were obtained from 5.5 g of cells.

Complex formation, grid freezing, and image processing

The purified ribosome sample (in buffer G) was filtered (0.22- μ m centrifugal filters, Millipore) and concentrated to a final concentration of ~1 to 2 mg/ml. Antibiotics were added at the following concentrations: 250 μ M for ANM and BLS, 100 μ M for PHY, and 1 mM for CHX. Aliquots of 2.7 μ l were applied to a freshly glow-discharged holey carbon grids (Quantifoil Cu R1.2/1.3 with ultrathin carbon support, 200 mesh), excess liquid was blotted away for 3 to 5 s using a FEI Vitrobot Mark IV (Thermo Fisher Scientific), and the samples were plunge-frozen in liquid ethane. Prepared grids were transferred into a Titan Krios 300-keV microscope (Thermo Fisher Scientific), equipped with a K3 direct electron detector or a Talos Arctica 200-keV microscope (Thermo Fisher Scientific), equipped with a K2 direct electron detector. Zero-loss images were recorded semiautomatically, using the UCSF Image script (14). The GIF Quantum energy filter was adjusted to a slit width of 20 eV. Images were collected at a various nominal magnification, yielding pixel sizes from 0.413 to 1.012 Å , and with a defocus range of -0.5 to -3.0 μ m. Movie images were collected with 24 frames dose-fractionated over 18 s. In total, we collected 9807, 2040, 2152, 1310, and 3199 micrographs for the vacant *C. albicans* ribosome or in complex with ANM, BLS, PHY, and CHX, respectively.

Motion correction, CTF (contrast transfer function) estimation, manual- and template-based particles picking, two-dimensional

(2D) classification, ab initio volume generation, CTF global and local refinements, and nonuniform 3D refinement were performed using cryoSPARC (v 3.1) (15). Maps were sharpened using Autosharpen Map procedure in Phenix (16). The separate masks for the focused refinement were generated for 60S and 40S subunits using Chimera. The cryo-EM data processing schemes for the vacant *C. albicans* ribosome and in complex with investigated inhibitors are presented in figs. S8 to S12, and local resolution maps are presented in fig. S13.

Modeling

The structure of the *S. cerevisiae* 80S ribosome (17) was used as a template for model building. Model-to-map alignment was performed in Chimera (18). The 60S and 40S subunits were refined separately into their respective focused refined maps using the Phenix real-space refinement (16). The protein and rRNA chains were visually checked in Coot (19) and manually adjusted where necessary. All investigated inhibitors were manually docked into the experimental density, followed by real-space refinement in Phenix (16). The 40S subunit of *C. albicans* follows a classic division into the head, body, and shoulder consisting of 1787 nucleotides (nt) in 18S rRNA and 32 ribosomal proteins. The 18S rRNA is 13 and 82 nt shorter than the 18S rRNA of *S. cerevisiae* and *H. sapiens*, respectively. The large subunit (LSU) contains an active peptidyl transferase site that catalyzes the formation of peptide bonds during protein synthesis. In *C. albicans*, this 60S subunit includes 25S rRNA (3361 nt), 5.8S rRNA (157 nt), 5S rRNA (121 nt), and 45 proteins. The 25S rRNA is 35 nt shorter than the 25S rRNA of *S. cerevisiae* and 1716 nt shorter than the 28S rRNA of *H. sapiens*. 5.8S rRNA and 5S rRNA are almost identical to that in *S. cerevisiae* and *H. sapiens* (only 5.8S is 1 nt shorter). The ribosomal proteins of the LSU of the *C. albicans* ribosome are highly identical (82%) to those in *S. cerevisiae* and *H. sapiens*. The exception is the eL40 protein that is more than twice as short [52 amino acids instead of 128 amino acids in *S. cerevisiae*]. The only unmodeled regions are the L1-stalk and the P-stalk. In addition, because of disordered density and high flexibility, the expansion segments and some protein loops were only partially built in our structures. Overall, the *C. albicans* ribosome model includes 95% of amino acids and 92% of RNA residues from the entire sequence. The model quality statistics are presented in tables S2 to S6.

Inhibition of cell-free translation by CHX, PHY, ANM, and BLS

We prepared CFTSs from the *C. albicans* and *S. cerevisiae* strains used for structural analyses. These CFTSs were programmed with LUC mRNA, and then their capacity to produce the enzyme in the presence of increasing concentrations of CHX was examined. *C. albicans* belongs to a subclade in which the “universal” genetic code is altered; in this “CTG-clade,” the CUG codon is translated as Ser, not Leu (20, 21). Therefore, spLUC was used as the translational reporter because the coding region for this enzyme lacks CUG codons and functions as a reporter in *C. albicans* (22). Translation of spLUC RNA using CFTSs from these yeasts can thus be directly compared without concern for their use of different genetic codes.

C. albicans and *S. cerevisiae* CFTSs were prepared using the method 1 protocol for *S. cerevisiae*, and translation reactions were assayed for LUC activity, as described in (23). Rabbit reticulocyte lysate (RRL) was obtained from Promega (L4960). Capped and polyadenylated spLUC mRNA was prepared by T7 transcription of

EcoRI-linearized plasmid pQQ101 encoding spLUC (24). For quantification, triplicate-independent CFTSs (10 μ l each) programmed with 60 ng of spLUC RNA and RRLs programmed with 6 ng of spLUC RNA were incubated at 26°C in the absence or presence of different concentrations of inhibitors for 30 min and the activity of spLUC then measured by luminometry.

Drug susceptibility assay

Drug susceptibility was determined as previously described with modifications (25). Briefly, twofold dilution series of CHX were prepared in fresh YPD medium and distributed into 96-well plates (Falcon, 351177). *C. albicans* and *S. cerevisiae* cells from overnight cultures grown in 3 ml of YPD medium were collected and resuspended in 500 μ l of fresh YPD medium. The numbers of cells were then determined using a hemocytometer. Cell suspensions were diluted with fresh YPD medium to make working suspensions of 2×10^3 cells per ml and distributed into the drug dilution series (volume ratio, 1:1) in the 96-well plates and mixed well. Plates were statically incubated at 30°C for 24 hours, and OD₆₀₀ was measured with a SpectraMax M2^e microplate spectrophotometer.

Figure preparation

Cryo-EM maps were manually inspected in Coot (19). Panels of figures showing structural models were prepared using PyMOL and Gimp. The sequence of logo drawings was made using WebLogo 3.7.4 (26).

Data deposition

The final models and associated maps are deposited with the PDB and Electron Microscopy Data Bank (EMDB) with the following accession codes: 7PZY and EMD-13737 for the vacant *C. albicans* ribosome, 7Q0P and EMD-13749 for complex with ANM, 7Q0R and EMD-13750 for complex with BLS, 7Q0F and EMD-13744 for complex with PHY, and 7Q08 and EMD-13741 for complex with CHX, respectively.

SUPPLEMENTARY MATERIALS

Supplementary material for this article is available at <https://science.org/doi/10.1126/sciadv.abn1062>

[View/request a protocol for this paper from Bio-protocol.](#)

REFERENCES AND NOTES

- F. L. Mayer, D. Wilson, B. Hube, *Candida albicans* pathogenicity mechanisms. *Virulence* **4**, 119–128 (2013).
- G. C. de Oliveira Santos, C. C. Vasconcelos, A. J. O. Lopes, M. d. S. de Sousa Cartágenes, A. K. D. B. Filho, F. R. F. do Nascimento, R. M. Ramos, E. R. R. B. Pires, M. S. de Andrade, F. M. G. Rocha, C. de Andrade Monteiro, *Candida* infections and therapeutic strategies: Mechanisms of action for traditional and alternative agents. *Front. Microbiol.* **9**, 1351 (2018).
- D. N. Wilson, The A-Z of bacterial translation inhibitors. *Crit. Rev. Biochem. Mol. Biol.* **44**, 393–433 (2009).
- D. Bruchlen, “*Candida albicans* ribosome: Structure, function and inhibition,” thesis, Strasbourg University, Strasbourg (2016).
- J. H. Bae, B. H. Sung, J. H. Sohn, Site saturation mutagenesis of ribosomal protein L42 at 56th residue and application as a consecutive selection marker for cycloheximide resistance in yeast. *FEMS Microbiol. Lett.* **365**, fny066 (2018).
- P. Dehoux, J. Davies, M. Cannon, Natural cycloheximide resistance in yeast. The role of ribosomal protein L41. *Eur. J. Biochem.* **213**, 841–848 (1993).
- R. Ben-Yaacov, S. Knoller, G. A. Caldwell, J. M. Becker, Y. Koltin, *Candida albicans* gene encoding resistance to benomyl and methotrexate is a multidrug resistance gene. *Antimicrob. Agents Chemother.* **38**, 648–652 (1994).
- S. Kawai, S. Murao, M. Mochizuki, I. Shibuya, K. Yano, M. Takagi, Drastic alteration of cycloheximide sensitivity by substitution of one amino acid in the L41 ribosomal protein of yeasts. *J. Bacteriol.* **174**, 254–262 (1992).
- N. Garreau de Loubresse, I. Prokhorova, W. Holtkamp, M. V. Rodnina, G. Yusupova, M. Yusupov, Structural basis for the inhibition of the eukaryotic ribosome. *Nature* **513**, 517–522 (2014).
- S. Pellegrino, M. Meyer, Z. A. Könst, M. Holm, V. K. Voora, D. Kashinskaya, C. Zanette, D. L. Mobley, G. Yusupova, C. D. Vanderwal, S. C. Blanchard, M. Yusupov, Understanding the role of intermolecular interactions between lissoclimides and the eukaryotic ribosome. *Nucleic Acids Res.* **47**, 3223–3232 (2019).
- L. Shen, K. Yang, C. Wu, T. Becker, D. Bell-Pedersen, J. Zhang, M. S. Sachs, Structure of the translating *Neurospora* ribosome arrested by cycloheximide. *Proc. Natl. Acad. Sci. U.S.A.* **118**, e2111862118 (2021).
- R. Buschauer, Y. Matsuo, T. Sugiyama, Y. H. Chen, N. Alhusaini, T. Sweet, K. Ikeuchi, J. Cheng, Y. Matsuki, R. Nobuta, A. Gilmozzi, O. Berninghausen, P. Tesina, T. Becker, J. Coller, T. Inada, R. Beckmann, The Ccr4-Not complex monitors the translating ribosome for codon optimality. *Science* **368**, eaay6912 (2020).
- M. S. Skrzypek, J. Binkley, G. Sherlock, Using the Candida Genome Database. *Methods Mol. Biol.* **1757**, 31–47 (2019).
- X. Li, S. Zheng, D. A. Agard, Y. Cheng, Asynchronous data acquisition and on-the-fly analysis of dose fractionated cryoEM images by UCSFImage. *J. Struct. Biol.* **192**, 174–178 (2015).
- A. Punjani, J. L. Rubinstein, D. J. Fleet, M. A. Brubaker, cryoSPARC: Algorithms for rapid unsupervised cryo-EM structure determination. *Nat. Methods* **14**, 290–296 (2017).
- D. Liebschner, P. V. Afonine, M. L. Baker, G. Bunkóczi, V. B. Chen, T. I. Croll, B. Hintze, L. W. Hung, S. Jain, A. J. McCoy, N. W. Moriarty, R. D. Oeffner, B. K. Poon, M. G. Prisant, R. J. Read, J. S. Richardson, D. C. Richardson, M. D. Sammito, O. V. Sobolev, D. H. Stockwell, T. C. Terwilliger, A. G. Urzhumtsev, L. L. Videau, C. J. Williams, P. D. Adams, Macromolecular structure determination using x-rays, neutrons and electrons: Recent developments in Phenix. *Acta Crystallogr. D Struct. Biol.* **75**, 861–877 (2019).
- A. Ben-Shem, N. Garreau de Loubresse, S. Melnikov, L. Jenner, G. Yusupova, M. Yusupov, The structure of the eukaryotic ribosome at 3.0 Å resolution. *Science* **334**, 1524–1529 (2011).
- E. F. Pettersen, T. D. Goddard, C. C. Huang, G. S. Couch, D. M. Greenblatt, E. C. Meng, T. E. Ferrin, UCSF Chimera—A visualization system for exploratory research and analysis. *J. Comput. Chem.* **25**, 1605–1612 (2004).
- A. Casanal, B. Lohkamp, P. Emsley, Current developments in Coot for macromolecular model building of electron cryo-microscopy and crystallographic data. *Protein Sci.* **29**, 1069–1078 (2020).
- P. Kammer, S. McNamara, T. Wolf, T. Conrad, S. Allert, F. Gerwien, K. Hünigler, O. Kurzai, R. Guthke, B. Hube, J. Linde, S. Brunke, Survival strategies of pathogenic *Candida* species in human blood show independent and specific adaptations. *MBio* **11**, e02435-20 (2020).
- K. E. Priestov, M. A. Ghannoum, Resistance of *Candida* to azoles and echinocandins worldwide. *Clin. Microbiol. Infect.* **25**, 792–798 (2019).
- T. Srikantha, A. Klapach, W. W. Lorenz, L. K. Tsai, L. A. Laughlin, J. A. Gorman, D. R. Soll, The sea pansy *Renilla reniformis* luciferase serves as a sensitive bioluminescent reporter for differential gene expression in *Candida albicans*. *J. Bacteriol.* **178**, 121–129 (1996).
- C. Wu, N. Amrani, A. Jacobson, M. S. Sachs, The use of fungal in vitro systems for studying translational regulation. *Methods Enzymol.* **429**, 203–225 (2007).
- Z. Wang, P. Fang, M. S. Sachs, The evolutionarily conserved eukaryotic arginine attenuator peptide regulates the movement of ribosomes that have translated it. *Mol. Cell. Biol.* **18**, 7528–7536 (1998).
- Subcommittee on Antifungal Susceptibility Testing (AFST) of the ESCMID European Committee for Antimicrobial Susceptibility Testing (EUCAST), EUCAST definitive document EDef 7.1: Method for the determination of broth dilution MICs of antifungal agents for fermentative yeasts. *Clin. Microbiol. Infect.* **14**, 398–405 (2008).
- G. E. Crooks, G. Hon, J. M. Chandonia, S. E. Brenner, WebLogo: A sequence logo generator. *Genome Res.* **14**, 1188–1190 (2004).
- W. H. Mager, R. J. Planta, J. G. Ballesta, J. C. Lee, K. Mizuta, K. Suzuki, J. R. Warner, J. Woolford, A new nomenclature for the cytoplasmic ribosomal proteins of *Saccharomyces cerevisiae*. *Nucleic Acids Res.* **25**, 4872–4875 (1997).
- N. F. Kaufer, H. M. Fried, W. F. Schwindinger, M. Jasin, J. R. Warner, Cycloheximide resistance in yeast: The gene and its protein. *Nucleic Acids Res.* **11**, 3123–3135 (1983).
- Z. Huang, K. Chen, J. Zhang, Y. Li, H. Wang, D. Cui, J. Tang, Y. Liu, X. Shi, W. Li, D. Liu, R. Chen, R. S. Curgang, X. Pan, A functional variomics tool for discovering drug-resistance genes and drug targets. *Cell Rep.* **3**, 577–585 (2013).
- J. L. Hansen, P. B. Moore, T. A. Steitz, Structures of five antibiotics bound at the peptidyl transferase center of the large ribosomal subunit. *J. Mol. Biol.* **330**, 1061–1075 (2003).

Acknowledgments: We thank the NIH/NCI Developmental Therapeutics Program for providing materials. We thank the curators at the Candida Genome Database (13) and Gavin Sherlock (Stanford University Medical School) for finding the sequence of eL41. We thank J. Rheinberger for the help with the preparation of EM grids. We thank personnel of NeCEN for the assistance with data collection. We thank M. Breuer for help with the figure preparation of cell-free assays. **Funding:** This work was supported by Russian Science Foundation grant

20-65-47031 (to S.V.), Russian Science Foundation grant 20-64-47041 (to A.G.), La Fondation pour la Recherche Médicale FDT202106012811 (to Y.Z.), NIH grant R21 AI138158 (to M.S.S.), La Fondation pour la Recherche Médicale DEQ20181039600 (to M.Y.), and La Fondation pour la Recherche Médicale DBF20160635745 (to G.Y.). The access to NeCEN facilities was funded by the Netherlands Electron Microscopy Infrastructure (NEMI), project number 184.034.014 of the National Roadmap for Large-Scale Research Infrastructure of the Dutch Research Council (NWO). **Author contributions:** Conceptualization: Y.Z., O.K., M.S.S., G.Y., A.G., and M.Y. Methodology: Y.Z., O.K., A.S., C.W., D.B., G.Y., M.S.S., A.G., and M.Y. Investigation: Y.Z., O.K., A.S., C.W., and L.J. Visualization: Y.Z., O.K., A.S., C.W., and L.J. Funding acquisition: Y.Z., K.U., S.V., A.R., M.S.S., A.G., G.Y., and M.Y. Project administration: M.S.S., A.G., M.Y., and G.Y. Supervision: M.S.S., A.G., M.Y., and G.Y. Writing—original draft: Y.Z., O.K., A.S., S.V., A.R., C.W., G.Y., M.S.S., A.G., and M.Y. Writing—review and editing: Y.Z., O.K., A.S., C.W., K.U., L.J., M.S.S., A.G., G.Y., and M.Y.

Competing interests: The authors declare that they have no competing interests. **Data and materials availability:** All data needed to evaluate the conclusions in the paper are present in the paper and/or the Supplementary Materials. Atomic coordinates and cryo-EM maps for the reported structures have been deposited in the PDB and EMDB under accession codes 7PZY and EMD-13737 for the vacant *C. albicans* ribosome, 7Q0P and EMD-13749 for complex with ANM, 7Q0R and EMD-13750 for complex with BLS, 7Q0F and EMD-13744 for complex with PHY, and 7Q08 and EMD-13741 for complex with CHX, respectively.

Submitted 3 November 2021

Accepted 7 April 2022

Published 25 May 2022

10.1126/sciadv.abn1062